Opto-Electronic Advances

Supplementary information

2021, Vol. 4, No. 9

DOI: 10.29026/oea.2021.210017

Light-triggered interfacial charge transfer and enhanced photodetection in CdSe/ZnS quantum dots/MoS_2 mixed-dimensional phototransistors

Ziwei Li*, Wen Yang, Ming Huang, Xin Yang, Chenguang Zhu, Chenglin He, Lihui Li, Yajuan Wang, Yunfei Xie, Zhuoran Luo, Delang Liang, Jianhua Huang, Xiaoli Zhu, Xiujuan Zhuang, Dong Li and Anlian Pan*

Key Laboratory for Micro-Nano Physics and Technology of Hunan Province, College of Materials Science and Engineering, School of Physics and Electronics, Hunan University, Changsha 410082, China.

*Correspondence: ZW Li, E-mail: ziwei_li@hnu.edu.cn; AL Pan, E-mail: anlian.pan@hnu.edu.cn

This file includes:

Supplementary information for this paper is available at https://doi.org/10.29026/oea.2021.210017

Section 1: Optical images of heterostructures

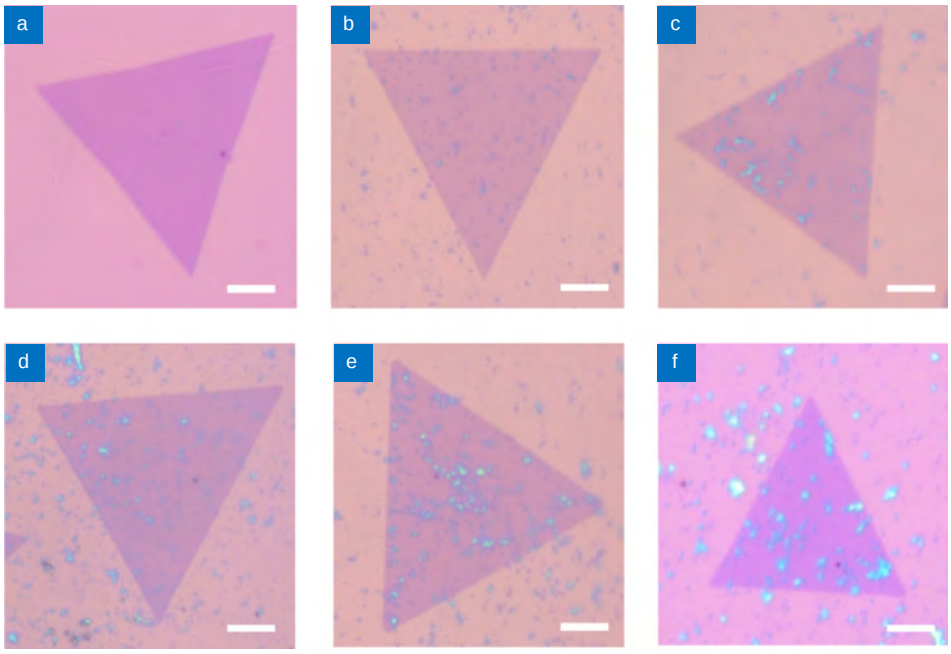

Fig. S1 | (**a**-**g**) shows the optical images of QD/MoS_2 heterostructures with the QD concentrations ranging from 0 mg/L, 0.05 mg/L, 0.1 mg/L, 0.4 mg/L, 0.8 mg/L, 1.6 mg/L. The optical properties were measured with a home-built μ-PL system. An iHR550 Raman spectrometer from Horiba was utilized to measure the PL and Raman spectra with 300 g mm^{-1} and 1200 g mm^{-1} gratings, respectively. A Ti: Sapphire laser at 400 nm (100 fs, 80 MHz) was used as the excitation source for transient measurements, which was generated by an 800 nm laser from a mode-locked oscillator (Tsunami 3941-X1BB, Spectra- Physics) positioned after a BBO crystal. Time-resolved PL (TRPL) is measured by a streak camera (Hasmamatsu Universal, C10910) with a resolution of ~3 ps for short-time range measurements (~200 ps). A 532 nm solid-state laser was introduced to excite the samples to obtain the steady-state spectra. The objective lens is 50× magnifications, and the diameter of the laser spot is ~2 μm.

Section 2: AFM images of heterostructures

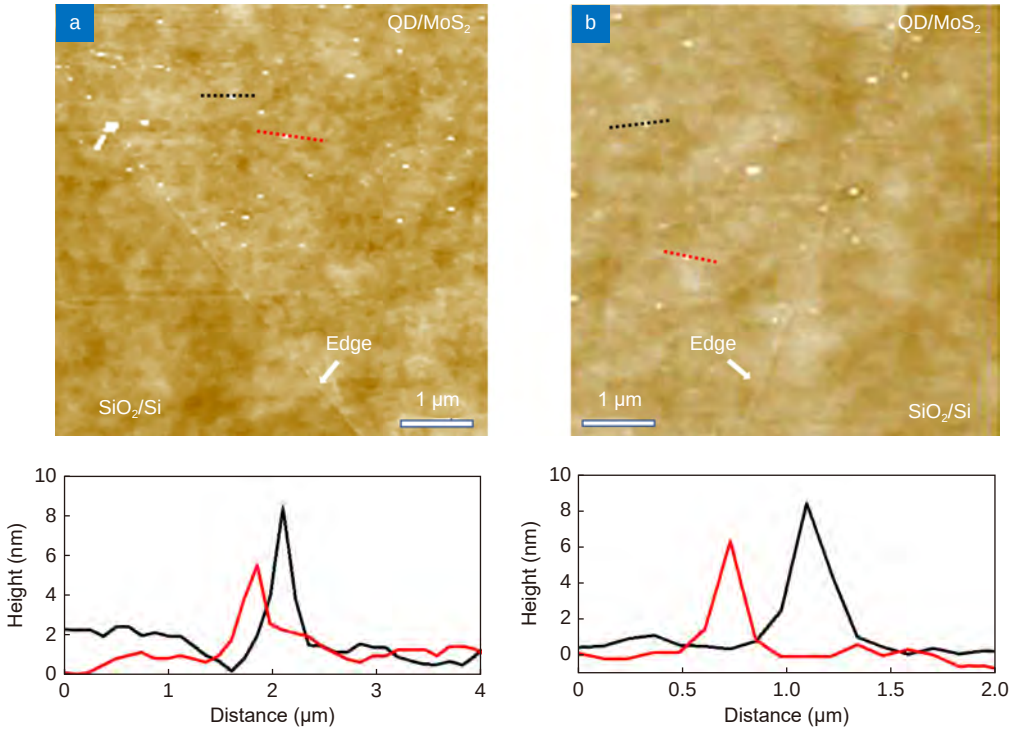

Fig. S2 | Shows the AFM images of QD/MoS_2 heterostructures with 0.05 mg/L and 0.025 mg/L QDs, respectively. The height profiles as noted as the dotted lines in AFM images show the height of QDs are 6−10 nm.

Section 3: Fitted lifetime of MoS_2 and heterostructures

The decay processes are considered to consist of fast decay τ_1 and slow decay τ_2. The fast decay is the related to trap-assisted recombination in QDs or carrier extraction by the layers in heterostructures, while the slow decay is related to radiative recombination. a_1 and a_2 are the ratios of the fast and the slow decay processes, respectively. When the interfacial charge transfer is induced, a_1 increases from 0.641 (QDs) to 0.857 (QD/MoS_2), while a_2 decreases from 0.359 (QDs) to 0.1429 (QD/MoS_2).

	τ_1(ps)	τ_2(ps)	a_1(%)	a_2(%)	$\tau_{average}$(ps)
QD_S	154.458	1090.75	0.641	0.359	490.5868
QD/MoS_2	53.805	369.23	0.8571	0.1429	98.87923

Section 4: Spectral evolution of heterostructures with various QD concentrations

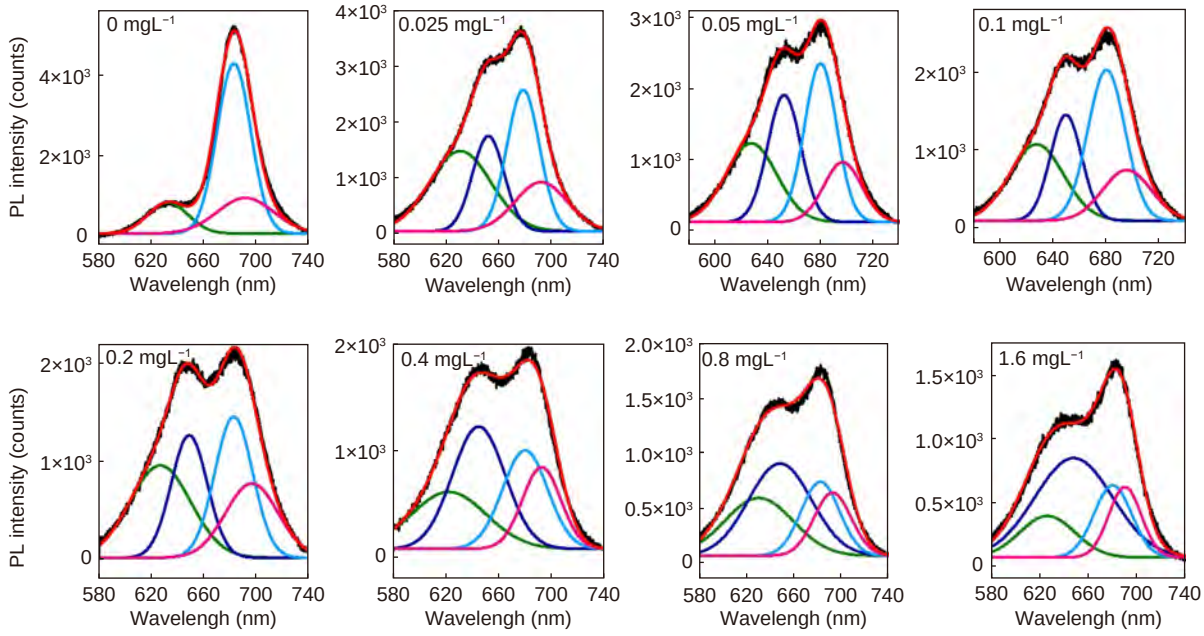

Fig. S4 | Shows the spectral evolution of heterotructures with various QD concentrations ranging from 0.025 to 3.2 mg/L, where fitting curves involve B exciton (green), A exciton (blue), trion (pink) and QD exciton (dark blue).

Section 5: The framework of a three energy level

The rate equations of exciton (A) and trion (A') can be expressed below,

$$\frac{\mathrm{d}N_A}{\mathrm{d}t} = G - \left[\Gamma_{\mathrm{ex}} + K_{\mathrm{tr}}(n)\right] N_A, \tag{1}$$

$$\frac{\mathrm{d}N_{A'}}{\mathrm{d}t} = K_{\mathrm{tr}}(n) N_A - \Gamma_{\mathrm{tr}} N_{A'}, \tag{2}$$

$$K_{\mathrm{tr}}(n) = K_{\mathrm{tr}}(0)\left(1 - s\frac{1}{\alpha \cdot n + 1}\right), \tag{3}$$

where N_A, $N_{A'}$ is the population of exciton and trion, n is the doping steps. Assuming that the rate of adsorption of QDs obey the Langmuir's law, the rate of formation of trion with doping steps can be described as $k_{\mathrm{tr}}(n)$. s (~95%) reflects the ability of charge transfer from a GQDs molecule to a single-layer MoS_2. δ is the concentration and α is a parameter that reflects the adsorption probability. The populations of exciton and trion can be derived from the steady-state functions as below

$$N_A(n) = \frac{G}{\Gamma_{\mathrm{ex}} + K_{\mathrm{tr}}(n)} \tag{4}$$

$$N_{A'}(n) = \frac{K_{\mathrm{tr}}(n)}{\Gamma_{\mathrm{tr}}} \frac{G}{\Gamma_{\mathrm{ex}} + K_{\mathrm{tr}}(n)} \tag{5}$$

where Γ_{ex} and Γ_{tr} represent the decay rates of exciton and trion, respectively. The PL intensity can be considered to be proportional to populations of the exciton and trion, expressed as

$$I_A(n) = \frac{BG\gamma_{\mathrm{ex}}}{\Gamma_{\mathrm{ex}} + K_{\mathrm{tr}}(n)} \tag{6}$$

$$I_{A'}(n) = \frac{K_{\mathrm{tr}}(n)}{\Gamma_{\mathrm{tr}}} \frac{BG\gamma_{\mathrm{tr}}}{\Gamma_{\mathrm{ex}} + K_{\mathrm{tr}}(n)} \tag{7}$$

where parameter B is the collection efficiency of luminescene, γ_{ex} and γ_{tr} represent the radiative rates of exciton and trion, respectively. In the consideration, the change of these values is assumed to be small and can be neglected during the doping process. Here, we suppose that the rate of radiative decay is independent of carrier density in our experiments for simplicity. The values Γ_{ex} = 0.002ps^{-1}, Γ_{tr} = 0.02ps^{-1} in the analysis are based on the values reported before. For simple condition that $k_{\mathrm{tr}} >> \Gamma_{\mathrm{i}}$ (i=ex, tr), the PL intensity can be approximately expressed as

$$I_A(n) \approx \frac{AG\gamma_{\mathrm{ex}}}{K_{\mathrm{tr}}(n)} \tag{8}$$

$$I_{A'}(n) \approx \frac{AG\gamma_{\mathrm{tr}}}{\Gamma_{\mathrm{tr}}} \tag{9}$$

Section 6: Mass action model

The mass action model associated with the trion is applied to calculate charge density of MoS_2. Under the law of mass action, the following function is obtained:

$$\frac{N_A n_{\mathrm{e}}}{N_{A'}} = \left(\frac{16\pi m_A m_{\mathrm{e}}}{h^2 m_{A-}}\right) k_{\mathrm{B}} T \exp\left(-\frac{E_{\mathrm{b}}}{k_{\mathrm{B}} T}\right) \tag{10}$$

where k_{B} is the Boltzman constant, T is the temperature, E_{b} is the binding energy of trions near the bandgap. The m_0 is the mass of a free electron, also m_{e} ($0.35m_0$) and m_{h} ($0.45m_0$) are the effective mass of electrons and holes, respectively. The effective masses of an exciton and a trion can be calculated as $m_A = 0.8m_0$, $m_{A'} = 1.15m_0$. Using these parameters, the weight of exciton A PL intensity can be expressed as

$$\frac{I_A}{I_{\mathrm{total}}} = \frac{1}{1 + \frac{\gamma_{\mathrm{tr}}}{\gamma_{\mathrm{ex}}} \frac{N_{A'}}{N_A}} \approx \frac{1}{1 + 2.2 \times 10^{-14} n_{\mathrm{el}}} \tag{11}$$

Section 7: Power-dependent fitting spectra of MoS_2

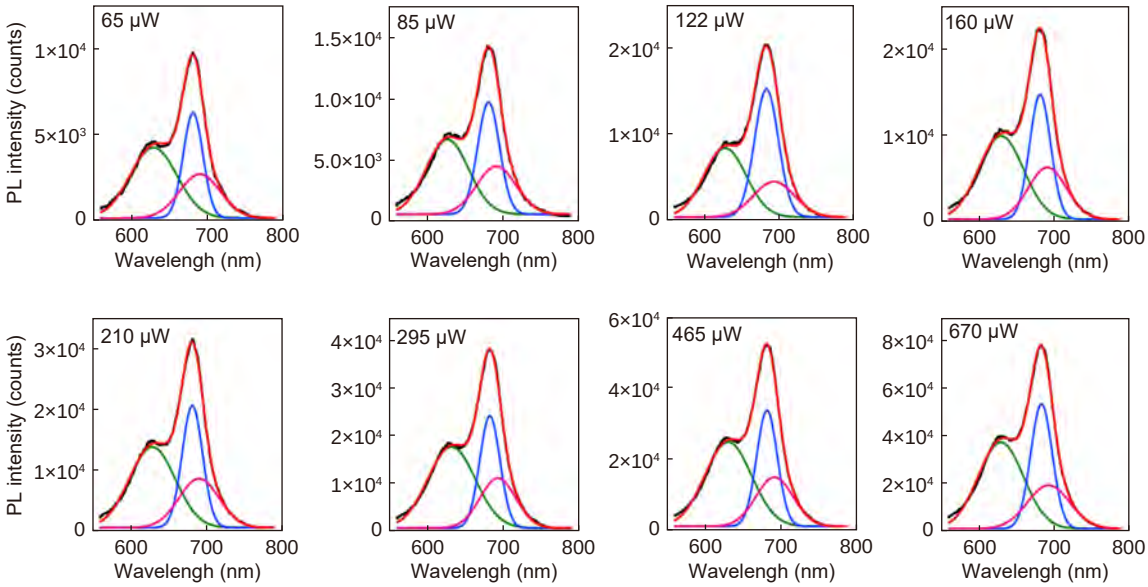

Fig. S5 | Shows the spectral evolution at various laser powers ranging from 65 to 670 μW, where fitting curves involve the components of exciton B (green), exciton A (blue) and trion (purple).

Section 8: Power-dependent fitting spectra of QD/MoS_2

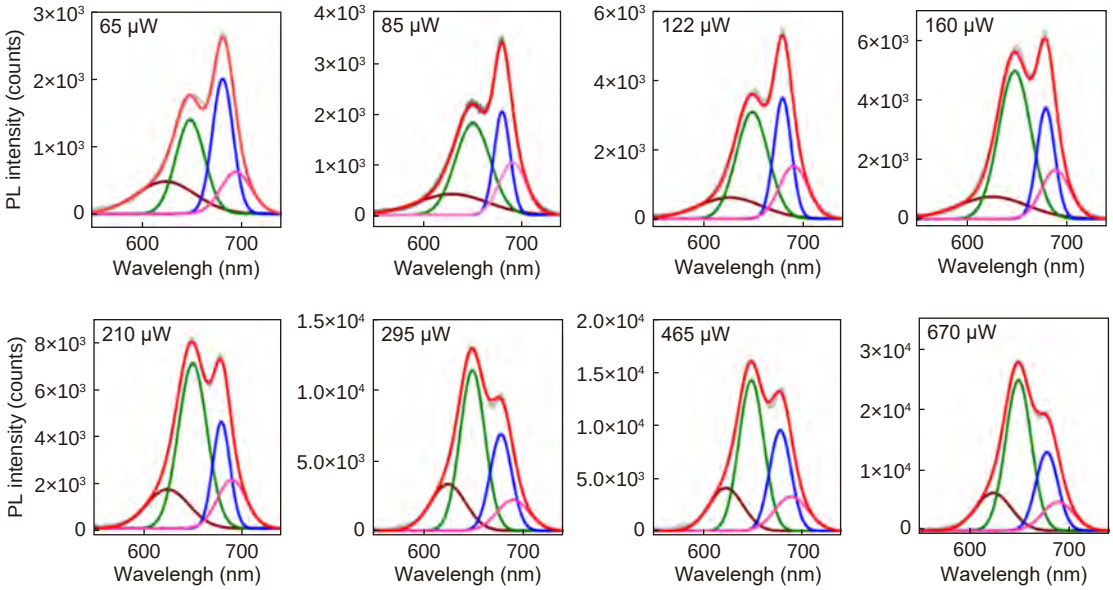

Fig. S6 | Shows the spectral evolution at various laser powers ranging from 65 to 670 μW, where fitting curves involve the components of exciton B (brown), exciton A (blue), trion (pink) and QD exciton (green).

Section 9: Carrier mobility of MoS_2 monolayer and QD/MoS_2 heterostructure

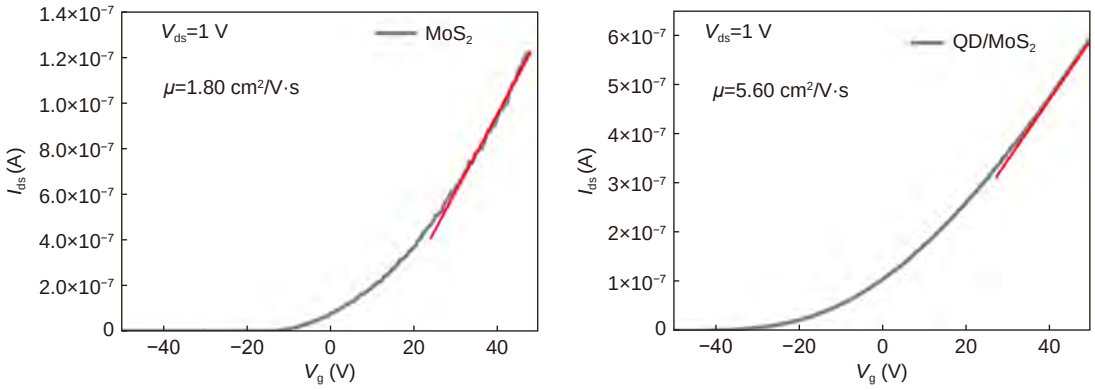

Fig. S7 | Shows the I_{ds}-V_g curves of MoS_2 monolayer and QD/MoS_2 heterostructure at V_{ds}=1 V, where the calculated carrier mobilities are 1.8 cm²/V·s and 5.6 cm²/V·s, respectively. Due the interfacial doping effect, the mobility of heterostructure device becomes more than three times larger than pure MoS_2 device. The metal electrodes of MoS_2 and heterostructure devices were fabricated in a typical E-beam lithography (EBL) process, followed by e-beam evaporation of Cr (5 nm) and Au (100 nm), respectively. Then, samples were annealed in vacuum for 3 h at ≈ 180 °C to improve the contact conductance. The surface ligands of the coated QDs were purified by ethyl acetate and hexane to facilitate charge transport. Finally, the devices were annealed on a hot plate at 50 °C for 10 min to evaporate the solvent for electrical measurements. The electrical and optoelectronic properties of the as-fabricated devices were performed in a vacuum Lake Shore Probe Station combined with an Agilent B1500A semiconductor analyzer at room temperature.

Section 10: Power-dependent photocurrents of MoS_2 monolayer and QD/MoS_2 heterostructure

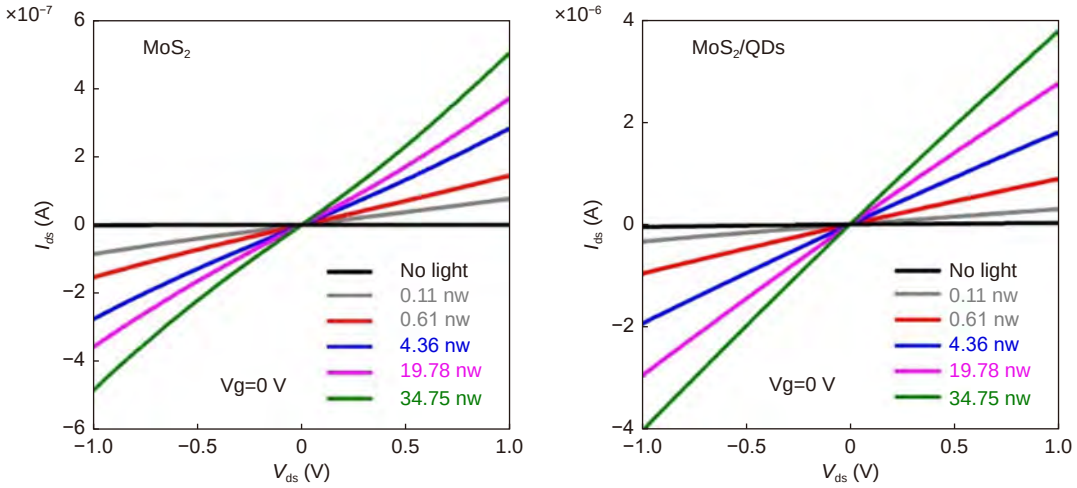

Fig. S8 | Shows the I_{ds}-V_{ds} curves of MoS_2 and QD/MoS_2 heterostructure under various illuminations.

Section 11: V_g-dependent optoelectronic device performances

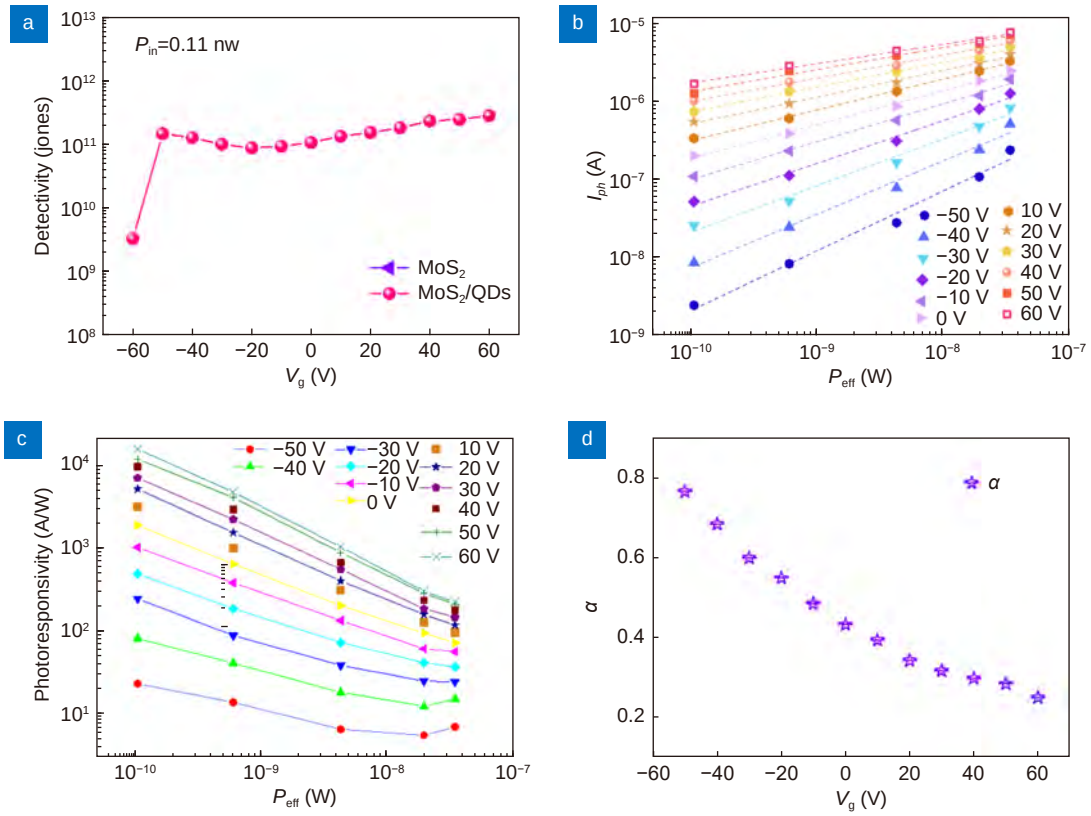

Fig. S9 | (**a**) V_g-dependent detectivities. (**b**) V_g-dependent I_{ph} at various illumination powers. (**c**) V_g-dependent R at various illumination powers. (**d**) V_g-dependent α. α decreases as V_g increases.

Section 12: Comparision of optoelectronic performance of QD/MoS_2 devices[1–7]

Heterostructure Device	Wavelength (nm)	Laser Power	V_g(V)	V_{ds}(V)	R (A/W)	D (Jones)	Ref.
$MoS_2/CH_3NH_3PbBr_3$ QDs	532	0.5 nw	60	1	3.72×10^3	2.0×10^{10}	1
$MoS_2/CsPbI_{3-x}Br_x$ QDs	532	0.5 nw	60	1	5.5×10^4	1.95×10^{12}	1
MoS_2/InP@ZnS QDs	532	34 mw/cm^2	40	1	1374		2
Bilayer-MoS_2/PbS QDs	635	13 mw/cm^2	−60	1	6×10^5	10^{11}	3
MoS_2/HgTe QDs	635	0.35 mw/cm^2	−15	1	5×10^3	6.4×10^{12}	4
$MoS_2/CsPbBr_3$ QDs	405	12.8 mw/cm^2	−20	1	4.68×10^4		5
MoS_2/CdSe QDs	580	37 mw	−40	0	400		6
MoS_2/ZnCdSe QDs	450	400 nw	0	1	3.7×10^4	1.0×10^{12}	7
Our work MoS_2/CdSe/ZnS QDs	520	0.11 nW	60	1	1.5×10^4	2.86×10^{11}	

References

1. Wu HL, Kang Z, Zhang ZH, Zhang Z, Si HN et al. Interfacial charge behavior modulation in perovskite quantum dot-monolayer MoS_2 0D-2D mixed-dimensional van der waals heterostructures. *Adv Funct Mater* **28**, 1802015 (2018).
2. Shi KX, Li JH, Xiao YC, Guo L, Chu XY et al. High-response, ultrafast-speed, and self-powered photodetection achieved in InP@ZnS-MoS_2 phototransistors with interdigitated Pt electrodes. *ACS Appl Mater Interfaces* **12**, 31382–31391 (2020).
3. Kufer D, Nikitskiy I, Lasanta T, Navickaite G, Koppens FHL et al. Hybrid 2D–0D MoS_2–PbS quantum dot photodetectors. *Adv Mater* **27**, 176–180 (2015).
4. Huo NJ, Gupta S, Konstantatos G. MoS_2–HgTe quantum dot hybrid photodetectors beyond 2 μm. *Adv Mater* **29**, 1606576 (2017).
5. Lin RC, Li XB, Zheng W, Huang F. Balanced photodetection in mixed-dimensional phototransistors consisting of $CsPbBr_3$ quantum dots and few-layer MoS_2. *ACS Appl Nano Mater* **2**, 2599–2605 (2019).
6. Li MX, Chen JS, Routh PK, Zahl P, Nam CY et al. Distinct optoelectronic signatures for charge transfer and energy transfer in quantum dot–MoS_2 hybrid photodetectors revealed by photocurrent imaging microscopy. *Adv Funct Mater* **28**, 1707558 (2018).
7. Zhang SK, Wang XD, Chen Y, Wu GJ, Tang YC et al. Ultrasensitive hybrid MoS_2–ZnCdSe quantum dot photodetectors with high gain. *ACS Appl Mater Interfaces* **11**, 23667–23672 (2019).